# Self-consistent projection operator theory in nonlinear quantum optical systems: A case study on degenerate optical parametric oscillators

Peter Degenfeld-Schonburg,[1,*] Carlos Navarrete–Benlloch,[2,†] and Michael J. Hartmann[3,‡]

[1]*Technische Universität München, Physik Department, James Franck Strasse, 85748 Garching, Germany*

[2]*Max-Planck-Institut für Quantenoptik, Hans-Kopfermann-strasse 1, 85748 Garching, Germany*

[3]*Institute of Photonics and Quantum Sciences, Heriot-Watt University, Edinburgh, EH14 4AS, United Kingdom*

Nonlinear quantum optical systems are of paramount relevance for modern quantum technologies, as well as for the study of dissipative phase transitions. Their nonlinear nature makes their theoretical study very challenging and hence they have always served as great motivation to develop new techniques for the analysis of open quantum systems. We apply the recently developed self-consistent projection operator theory to the degenerate optical parametric oscillator to exemplify its general applicability to quantum optical systems. We show that this theory provides an efficient method to calculate the full quantum state of each mode with a high degree of accuracy, even at the critical point. It is equally successful in describing both the stationary limit and the dynamics, including regions of the parameter space where the numerical integration of the full problem is significantly less efficient. We further develop a Gaussian approach consistent with our theory, which yields sensibly better results than the previous Gaussian methods developed for this system, most notably standard linearization techniques.

## I. INTRODUCTION

Nonlinear optical systems play an important role in the field of optics both in classical [1,2] and in quantum [3–8] regimes. Quantum mechanical effects, in particular, which are not explainable by classical optics, have triggered substantial research, especially in connection to modern applications such as high-precision measurements [9–12] and quantum information communication and processing [13–15]. Importantly, the nonlinear nature of these systems leads to non-Gaussian states, which typically precludes an analytic treatment and therefore requires elaborate theoretical approaches [16,17].

In a system where the dynamical degrees of freedom evolve on different time scales, approximate descriptions of reduced complexity may be found. For example, *adiabatic elimination* techniques can be exploited to derive effective equations of motion [18,19]. In this work, we apply the recently introduced *self-consistent projection operator theory* [20] to the *degenerate optical parametric oscillator*, and exemplify how it generalizes adiabatic elimination approaches. This theory takes dynamical backaction between the degrees of freedom into account and therefore does not require any time-scale separation. We expect our method to be directly applicable to other nonlinear quantum optical models such as those for nondegenerate or multimode parametric oscillation [8,21–24], lasing [3,4,25,26], optomechanical parametric oscillation [27,28], or the dissipative *Dicke model* [29–31].

Degenerate optical parametric oscillators (DOPOs) have been extensively studied in the past [5,8,17] and are one of the paradigm examples of a system subject to a driven and dissipative phase transition. It is formulated as a bosonic problem with two modes, *signal* and *pump*, subject to dissipation and interacting nonlinearly. In the adiabatic limit of a fast decaying pump mode, an effective master equation can be derived by means of standard projection operator approaches [17] and, due to its reduced complexity, the steady state can be found by solving the corresponding Fokker-Planck equations for the positive *P* distribution [32,33]. Yet away from the adiabatic limit, one has to resort to numerical simulations or perturbative treatments [34–39]. Nonequilibrium many-body techniques such as the Keldysh formalism have also been employed to study steady-state properties [40–42]. While the application of all of these techniques has deepened our understanding of DOPOs and phase transitions in driven-dissipative quantum systems enormously, it is important to note that they are naturally built to determine the evolution of observables, making the determination of the quantum state of the optical fields very challenging, if not impossible.

Our approach, in contrast, derives a set of coupled equations for the reduced states of the two optical modes of the DOPO. By numerically solving these equations, we find the reduced density matrices of both the pump and the signal modes. We test the accuracy of our method by comparing its results with those of the full DOPO problem in regions of the parameter space which are numerically tractable. Our findings show that our method is remarkably close to the exact results, both for steady states and dynamics, while being less numerically demanding than the full simulation of the DOPO problem. It thus gives access to the reduced states of the cavity modes in regions of the parameters that are inaccessible to the latter.

The possibly largest reduction of complexity in nonlinear quantum optical systems, however, comes from the application of Gaussian approximations on the state of the system. Within a Gaussian theory, one can basically cover the whole parameter space efficiently to determine both steady-state and dynamical quantities such as two-time correlation functions. The simplest and most widely used Gaussian approach is known as the *linearization technique* [32,43], which consists of assuming that the system configuration is, on average, in its classical state, but is constantly driven out of it by some "small" quantum fluctuations. While this technique provides a good

*peter.degenfeld-schonburg@ph.tum.de

†carlos.navarrete@mpq.mpg.de

‡m.j.hartmann@hw.ac.uk

qualitative picture of the physics in many, albeit not all, systems, it leads to unphysical predictions close to the critical points of the classical theory, e.g., to infinite photon numbers in the case of the DOPO [44]. These unphysical predictions can be regularized by applying a more elaborate Gaussian state approximation where the system is not forced to stay in its classical state, but chooses instead an average configuration more consistent with the quantum fluctuations that perturb it [45]. Motivated by such an idea, we apply a Gaussian approximation within the self-consistent projection operator theory and show that it gives more accurate quantitative results than any of the usual Gaussian techniques, as it does not assume a Gaussian state for the entire system, but only for the reduced state of one of the modes.

The remainder of the paper is organized as follows. In Sec. II, we introduce the DOPO model. We also discuss its symmetries and briefly elaborate on the standard linearization approach in Sec. II. Section III reviews the main concepts of the self-consistent projection operator theory and introduces the *self-consistent Mori-projector* (c-MoP) equations, which lie at the center of our study. Our theory provides a systematic extension of mean-field approaches, as demonstrated in Sec. III A, and reproduces known results in the *adiabatic* and the *diabatic* limits, introduced in Sec. III C. An efficient procedure designed to deal with the *non-Markovian* structure of the c-MoP equations is provided in Sec. III B, which we use in Sec. IV to test the accuracy of our method for steady-state quantities and to present quantum states of the signal mode. A Gaussian state approximation on the c-MoP equations is performed in Sec. V, which is shown to lead to highly accurate quantitative results as compared to previous linearization techniques. As a further test, we check in Sec. VI that our method provides the same level of accuracy for the dynamics as it does for steady states. Finally, we conclude our work and present an outlook in Sec. VII.

## II. THE DEGENERATE OPTICAL PARAMETRIC OSCILLATOR

A DOPO consists of a driven optical cavity containing a crystal with second-order optical nonlinearity; see Fig. 1. Two relevant resonances at frequencies $\omega_s$ (*signal* mode) and $\omega_p = 2\omega_s$ (*pump* mode) exist in the cavity, which are nonlinearly coupled via *parametric down-conversion* inside the crystal, capable of transforming a pump photon into a pair of signal photons, and vice versa. We assume that the external driving laser is resonant with the pump mode. By including damping through the partially transmitting mirrors at rates $\gamma_p$ and $\gamma_s$ for the pump and signal modes, respectively, the equation governing the evolution of the state $\rho$ of the system in a picture rotating at the laser frequency is given by [5,8,17]

$$\dot{\rho}(t) = \left[ \epsilon_p(a_p^\dagger - a_p) + \frac{\chi}{2}\left(a_p a_s^{\dagger 2} - a_p^\dagger a_s^2\right), \rho(t) \right]$$
$$+ \sum_{j=s,p} \gamma_j [2a_j \rho(t) a_j^\dagger - a_j^\dagger a_j \rho(t) - \rho(t) a_j^\dagger a_j], \quad (1)$$

where $\chi/2$ is the down-conversion rate and $\epsilon_p$ is proportional to the square root of the injected laser's power. We have defined bosonic operators $a_p$ and $a_s$ for the pump and signal modes, respectively, which satisfy canonical commutation
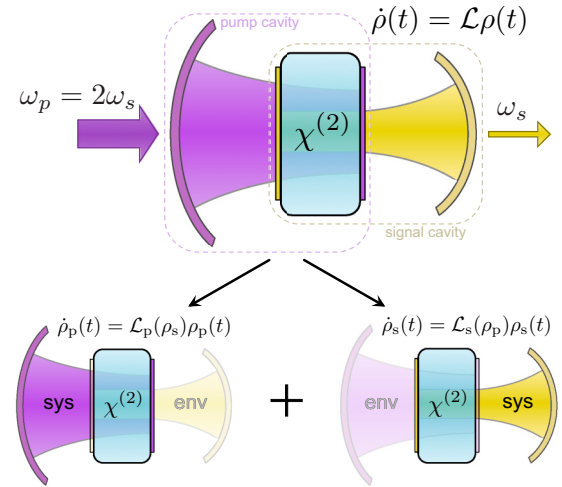


FIG. 1. (Color online) Sketch of the self-consistent projection operator theory for the DOPO, which consists of an optical cavity containing a crystal with second-order optical nonlinearity, pumped by a laser at frequency $\omega_p = 2\omega_s$ (pump mode), and capable of producing a field at the subharmonic frequency $\omega_s$ (signal mode) via down-conversion in the crystal. For the sake of illustration, we consider in the figure a doubly resonant semimonolithic configuration in which each face of the crystal acts as a mirror for one of the modes, but is transparent for the other, allowing the creation of independent cavities for the pump and signal modes via two additional partially transmitting mirrors [48]. In our approach, the full problem described by the state $\rho(t)$ and the Liouvillian $\mathcal{L}$ is mapped onto two coupled equations for the signal and pump modes. In one of the equations, the signal mode considered as the system is described by an effective master equation for its reduced state $\dot{\rho}_s(t) = \mathcal{L}_s(\rho_p)\rho_s(t)$ with an effective Liouvillian depending on the state of the pump, which plays here the role of an environment. The other equation considers the reversed scenario with the pump taking the role of the system while the signal is interpreted as the environment, leading to the effective equation $\dot{\rho}_p(t) = \mathcal{L}_p(\rho_s)\rho_p(t)$. In this way, the two equations form a closed set.

relations $[a_j, a_l^\dagger] = \delta_{jl}$ and $[a_j, a_l] = 0$. Note that the nonlinear interaction is third order in the field operators, precluding a general analytic solution of Eq. (1) which we refer to as the *Liouville–von Neumann equation* or simply the *full master equation* of the DOPO.

### Linearization approach and symmetry breaking

The right-hand side of Eq. (1) can also be written in a shorthand notation by introducing a superoperator $\mathcal{L}$ (*Liouvillian*), such that $\dot{\rho}(t) = \mathcal{L}\rho(t)$. For the major part of this work, we will be interested in the steady state $\rho_{ss} = \lim_{t\to\infty} \rho(t)$, which fulfills the equation $\mathcal{L}\rho_{ss} = 0$. Due to the dissipation acting on both modes and because an arbitrarily large but finite truncation will always provide an arbitrarily good approximation, we expect the steady state to be unique [46,47].

We further note the invariance of the Liouvillian under a unitary transformation $U_2$ of Ising-type $Z_2$ which transforms $a_s$ as $U_2 a_s U_2^\dagger = -a_s$. Since the steady state is unique, this implies that it has to be invariant under the $Z_2$ transformation too, i.e., $U_2 \rho_{ss} U_2^\dagger = \rho_{ss}$. This in turn leads to vanishing steady-state

expectation values which include odd powers of the signal field operator $a_s$. In particular, $\langle a_s \rangle = 0 = \langle a_p a_s^\dagger \rangle$, as, for example, $\langle a_s \rangle = \text{Tr}\{a_s \rho_{ss}\} = \text{Tr}\{U_2 a_s U_2^\dagger U_2 \rho_{ss} U_2^\dagger\} = -\langle a_s \rangle$.

However, the most common technique used to analyze Eq. (1), known as the *linearization approach*, breaks this $Z_2$ symmetry [32,43], which has to be restored "by hand" at the end of the calculation, following the procedure that we explain at the end of Sec. IV. Even though this method is more naturally introduced in the Heisenberg picture using the language of quantum Langevin equations, it also admits a Schrödinger picture interpretation in terms of two successive approximations in the master equation. It starts by writing the bosonic operators as $a_j = \alpha_j + \delta a_j$, with $\alpha_j = \langle a_j \rangle$ and, hence, $\langle \delta a_j \rangle = 0$. In the first approximation, the fluctuation operators $\delta a_j$ are neglected altogether; the evolution equations for $\langle a_j \rangle$ (Bloch equations) then provide a set of nonlinear differential equations for the amplitudes $\alpha_j$, which in the case of the DOPO read

$$
\begin{aligned}
\dot\alpha_p &= \epsilon_p - \gamma_p \alpha_p - \frac{\chi}{2}\alpha_s^2, \\
\dot\alpha_s &= -\gamma_s \alpha_s + \chi \alpha_p \alpha_s^*.
\end{aligned}
\tag{2}
$$

These correspond to the classical equations of the system, as they could have been obtained directly from Eq. (1) by assuming a coherent state for $\rho_{ss}$ or simply from Maxwell's equations. Depending on the *injection parameter* $\sigma = \chi\epsilon_p / \gamma_s\gamma_p$, one finds two types of steady-state solutions of Eq. (2). One of them has $\alpha_s = 0$ and $\alpha_p = \epsilon_p / \gamma_p$, and hence it does not break the symmetry; it is known as the *below-threshold solution* and is only stable for $\sigma < 1$. The other solution is phase bistable and has $\chi\alpha_s = \pm\sqrt{2(\chi\epsilon_p - \gamma_s)}$ and $\chi\alpha_p = \gamma_s$, hence breaking the $Z_2$ symmetry; it is known as the *above-threshold solution* and exists only for $\sigma > 1$. The threshold point $\sigma = 1$ marks a *critical point* where the classical theory predicts a phase transition from a signal-off phase with $\alpha_s = 0$ to a signal-on phase with $\alpha_s \neq 0$. In the signal-off phase, all injected power $\epsilon_p$ goes into the pump mode, while after crossing the critical point all the extra injection is transferred to the signal mode; see the gray thin solid line in Fig. 2.

Once the classical solutions have been identified, the second approximation consists of coming back to the original master equation with the bosonic operators written as $a_j = \alpha_j + \delta a_j$, and neglecting any term which goes beyond quadratic order in the fluctuation operators $\delta a_j$. This leads to a so-called *linearized master equation* which can be easily solved.

One has to keep in mind that this linearized theory can only be trustworthy when the classical solution is a strong attractor because only then are the quantum fluctuations driving the system out of equilibrium strongly damped, and quantum noise can be treated as a small perturbation. This means that, in particular, any predictions obtained through this method cannot be trusted in the vicinities of critical points of the classical theory: points of the parameter space where one solution becomes unstable, making way for a new solution to kick in, hence creating nonanalytic behavior in some observable, that is, a classical *phase transition*. Indeed, this is exactly the case for the DOPO, in which this linearized description breaks down at threshold, offering unphysical

predictions such as infinite photon numbers in the signal field (as illustrated by the gray thin line in Fig. 4).

## III. SELF-CONSISTENT MORI-PROJECTOR APPROACH

To explain the approach employed in our calculations, we will first recapitulate some basic ideas of the self-consistent projection operator theory [20]. The first step is to divide the entire system into subsystems. In the DOPO, this naturally amounts to consider the pump mode described by its reduced state $\rho_p(t) \equiv \text{Tr}_s\{\rho(t)\}$ and the signal mode described by $\rho_s(t) \equiv \text{Tr}_p\{\rho(t)\}$. In the spirit of *open system theory* [26,49], we will first treat the pump mode as an "environment" for the signal mode, which then takes the role of the open "system." Technically, this is done by introducing the time-dependent, self-consistent Mori projector $\mathcal{P}_t^p(\cdot) = \rho_p(t) \otimes \text{Tr}_p\{\cdot\}$ whose action on the full state $\rho(t)$ gives the factorized state $\mathcal{P}_t^p\rho(t) = \rho_p(t) \otimes \rho_s(t)$. The term "self-consistent" is chosen because the state of the pump in $\mathcal{P}_t^p$ is not a time-independent reference state, but is rather obtained consistently from the time-evolving state $\rho(t)$ of the full dynamics. Using this projector, we derive a generalized *Nakajima-Zwanzig* equation, which is an exact equation for the reduced state of the signal mode [20]. The effective Liouvillian describing such a Nakajima-Zwanzig equation will depend on the state of the pump $\rho_p(t)$. In order to obtain a closed set of equations, we need to reverse the scenario and treat the pump mode as the system and the signal mode as the environment; see Fig. 1 for an illustration.

Again analogous to open system theory, we split the full Liouvillian $\mathcal{L}$ from Eq. (1) into three parts. After performing a displacement $a_p \to a_p + \tilde\alpha_p$, where $\tilde\alpha_p$ will be chosen later (see Sec. III A), we write $\mathcal{L} = \mathcal{L}_p + \mathcal{L}_s + \mathcal{L}_I$, with

$$
\begin{aligned}
\mathcal{L}_p(\cdot) &= [a_p^\dagger(\epsilon_p - \gamma_p\tilde\alpha_p) - a_p(\epsilon_p - \gamma_p\tilde\alpha_p^*), (\cdot)] + \gamma_p D_{a_p}(\cdot), \\
\mathcal{L}_s(\cdot) &= \frac{\chi}{2}[\tilde\alpha_p a_s^{\dagger 2} - \tilde\alpha_p^* a_s^2, (\cdot)] + \gamma_s D_{a_s}(\cdot), \\
\mathcal{L}_I(\cdot) &= \frac{\chi}{2}[a_p a_s^{\dagger 2} - a_p^\dagger a_s^2, (\cdot)],
\end{aligned}
\tag{3}
$$

where we have defined the standard Lindblad superoperator $\mathcal{D}_b(\cdot) = 2b(\cdot)b^\dagger - b^\dagger b(\cdot) - (\cdot)b^\dagger b$, with $b$ being an arbitrary operator. The displacement $a_p \to a_p + \tilde\alpha_p$ moves the large coherent background of the pump field into the free evolution of the signal $\mathcal{L}_s$, keeping only the pump mode's fluctuations within the nonlinear signal-pump interaction $\mathcal{L}_I$. Such a step is important as our theory expands in powers of the interaction Liouvillian $\mathcal{L}_I$ in order to solve the Nakajima-Zwanzig equation. As in Ref. [20], we will expand to second order in the system-environment interaction. This approximation is known as the *Born approximation* [26]. Then, projecting the master equation $\dot\rho = \mathcal{L}\rho$ onto $\mathcal{P}_t^j$ and its complement $1 - \mathcal{P}_t^j$ ($j = s, p$), and formally integrating the latter considering the Born approximation, we get the following effective equations for the states of the signal and pump modes:

$$
\begin{aligned}
\dot\rho_s(t) &= \mathcal{L}_s\rho_s(t) + \frac{\chi}{2}\big[a_s^{\dagger 2}\langle a_p\rangle(t) - a_s^2\langle a_p\rangle^*(t), \rho_s(t)\big] \\
&\quad + \left(\frac{\chi}{2}\right)^2\left\{\left[a_s^2, \int_0^t dt' e^{\mathcal{L}_s(t-t')}\mathcal{K}_s(t,t')\rho_s(t')\right] + \text{H.c.}\right\},
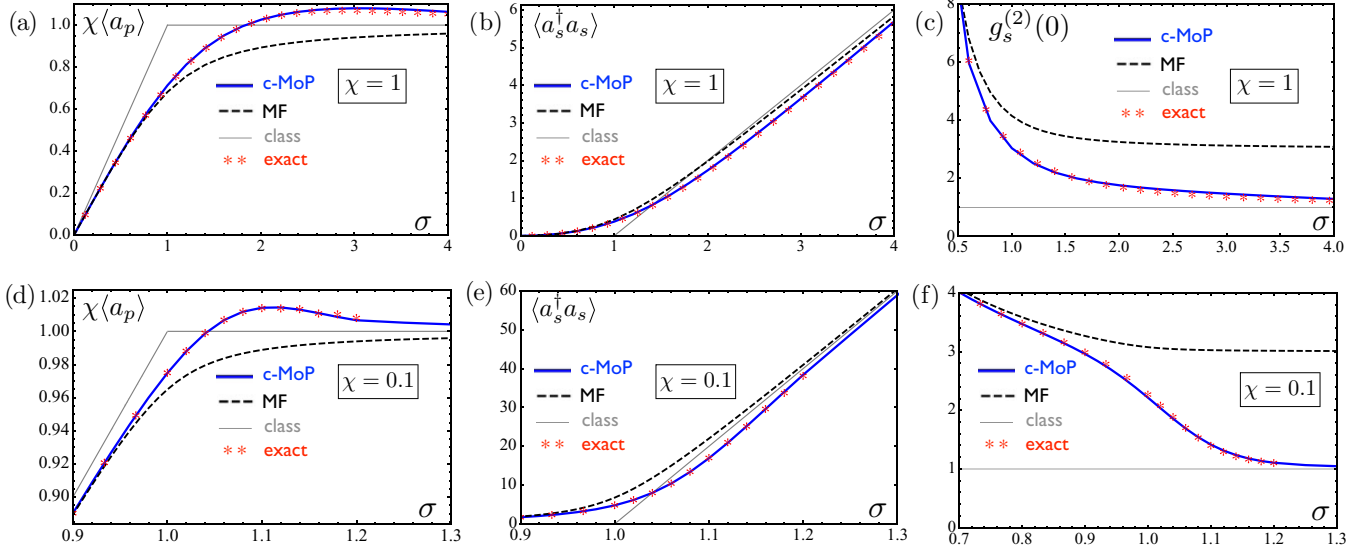\end{aligned}
\tag{4}
$$

FIG. 2. (Color online) Accuracy tests of the c-MoP theory for steady-state expectation values as a function of the injection parameter $\sigma$. In all plots, we set $\gamma_p = \gamma_s = 1$. The cases $\chi = 1$ and $\chi = 0.1$ are considered in (a)–(c) and (d)–(f), respectively. The rescaled pump amplitude $\chi\langle a_p \rangle$ is shown in (a) and (d); (b) and (e) show the signal photon number $\langle a_s^\dagger a_s \rangle$; finally, (c) and (f) show the $g^{(2)}$ function of the signal, which is equal to 1 for a coherent state (or a balanced mixture of coherent states differing only in phase). The gray thin solid lines show the classical prediction from Eq. (2), showing that the classical threshold where the signal field is switched on lies at $\sigma = 1$. The blue solid curves represent the results obtained from the numerical solution of the c-MoP equations (16), (17), (19), and (20). The red stars show the result obtained from the full master equation (1) up to injection parameters $\sigma$ where the numerics are tractable for us. Finally, the black dashed curves represent the mean-field theory; see Eq. (10). Apart from the classical solution, all theories conserve the $Z_2$ symmetry, i.e., $\langle a_s \rangle = 0$.

$$\dot{\rho}_p(t) = \mathcal{L}_p \rho_p(t) + \frac{\chi}{2}\big[a_p\langle a_s^2\rangle^*(t) - a_p^\dagger\langle a_s^2\rangle(t), \rho_p(t)\big]$$
$$+ \left(\frac{\chi}{2}\right)^2 \left\{\left[a_p, \int_0^t dt' e^{\mathcal{L}_p(t-t')}\mathcal{K}_p(t,t')\rho_p(t')\right] + \text{H.c.}\right\}, \tag{5}$$

where we have defined the kernel superoperators,

$$\mathcal{K}_s(t,t')(\cdot) = \delta a_s^2(t')(\cdot)\, d_p^+(t,t') - (\cdot)\delta a_s^2(t')\, \tilde{d}_p^+(t,t')$$
$$- \delta a_s^{\dagger 2}(t')(\cdot)\, d_p^-(t,t') + (\cdot)\delta a_s^{\dagger 2}(t')\, \tilde{d}_p^-(t,t'), \tag{6}$$

$$\mathcal{K}_p(t,t')(\cdot) = \delta a_p(t')(\cdot)\, d_s^+(t,t') - (\cdot)\delta a_p(t')\, \tilde{d}_s^+(t,t')$$
$$- \delta a_p^\dagger(t')(\cdot)\, d_s^-(t,t') + (\cdot)\delta a_p^\dagger(t')\, \tilde{d}_s^-(t,t'), \tag{7}$$

and for any operator $A_j$ acting on the signal $(j = s)$ or pump $(j = s)$ subspace, we have defined the corresponding fluctuation operator $\delta A_j(t) \equiv A_j - \text{Tr}_j\{A_j\, \rho_j(t)\}$.

The state of the pump mode $\rho_p(t)$ enters the signal mode's dynamics, given by Eq. (4), via $\langle a_p \rangle(t) \equiv \text{Tr}_p\{a_p \rho_p(t)\}$ and the correlation functions

$$d_p^+(t,t') = \text{Tr}_p\{a_p^\dagger e^{\mathcal{L}_p(t-t')}\delta a_p^\dagger(t')\rho_p(t')\},$$
$$\tilde{d}_p^+(t,t') = \text{Tr}_p\{a_p^\dagger e^{\mathcal{L}_p(t-t')}\rho_p(t')\delta a_p^\dagger(t')\},$$
$$d_p^-(t,t') = \text{Tr}_p\{a_p^\dagger e^{\mathcal{L}_p(t-t')}\delta a_p(t')\rho_p(t')\},$$
$$\tilde{d}_p^-(t,t') = \text{Tr}_p\{a_p^\dagger e^{\mathcal{L}_p(t-t')}\rho_p(t')\delta a_p(t')\}. \tag{8}$$

In turn, the state of the signal mode $\rho_s(t)$ enters the pump mode's dynamics, given by Eq. (5), via the expectation value

$\langle a_s^2 \rangle(t) \equiv \text{Tr}_s\{a_s^2 \rho_s(t)\}$ and the correlation functions

$$d_s^+(t,t') = \text{Tr}_s\{a_s^{\dagger 2} e^{\mathcal{L}_s(t-t')}\delta a_s^{\dagger 2}(t')\rho_s(t')\},$$
$$\tilde{d}_s^+(t,t') = \text{Tr}_s\{a_s^{\dagger 2} e^{\mathcal{L}_s(t-t')}\rho_s(t')\delta a_s^{\dagger 2}(t')\},$$
$$d_s^-(t,t') = \text{Tr}_s\{a_s^{\dagger 2} e^{\mathcal{L}_s(t-t')}\delta a_s^2(t')\rho_s(t')\},$$
$$\tilde{d}_s^-(t,t') = \text{Tr}_s\{a_s^{\dagger 2} e^{\mathcal{L}_s(t-t')}\rho_s(t')\delta a_s^2(t')\}. \tag{9}$$

Equations (4) and (5) should be understood as two coupled equations which represent effective equations for the reduced states of the signal and the pump mode. We refer to these two equations as the consistent Mori-projector (c-MoP) equations of the DOPO. They can be thought of as *non-Markovian* and *nonlinear master equations* which do not rely on any time-scale separation between the modes. We will elaborate in detail in Sec. III C on the limits where time-scale separation is present.

The only assumptions made so far are the Born approximation and the assumption of an initially factorized state $\rho(0) = \rho_p(0) \otimes \rho_s(0)$. The latter seems very reasonable by considering the vacuum as the state of the two modes before the driving laser is switched on. We also emphasize that our approach does not ignore system-environment or rather signal-pump correlations. In fact, it has been shown [20] that the *Born term*, the term second order in $\mathcal{L}_I$ which is proportional to $(\chi/2)^2$ here, clearly takes signal-pump correlations into account. We will show the crucial importance of the Born term in several examples below. Of course, c-MoP theory or any theory based on the concept of projection operators does not give access to explicit expressions for system-environment

correlation functions. An example in this context could be the cross-correlation function $\langle a_p^\dagger a_s \rangle - \langle a_p^\dagger \rangle \langle a_s \rangle$.

The most striking advantage of projection operator theories and, in particular, the c-MoP theory is the reduction of the complexity of the problem. In the example of the DOPO, the complexity of the Liouville–von Neumann equation (1) scales as $\dim \mathcal{H}_s \times \dim \mathcal{H}_p$, where $\mathcal{H}_{s/p}$ denotes the Hilbert space of the signal and pump modes, while the complexity of the c-MoP equations scale as $\dim \mathcal{H}_s + \dim \mathcal{H}_p$. The self-consistent Mori-projector theory thus offers a very significant reduction of complexity.

### A. Mean-field approximation

A merely approximate but very simple way of solving the c-MoP equations is to consider all terms up to first order in the interaction $\mathcal{L}_I$ only. Hence we drop all terms proportional to $\chi^2$ from Eqs. (4) and (5). Within this approximation, it does not make a difference whether or not the pump field is displaced. For simplicity, we put the displacement $\tilde\alpha_p$ from Eq. (3) to zero and obtain two coupled equations,

$$\dot\rho_p(t) = \left[ \left( \epsilon_p - \frac{\chi}{2}\langle a_s^2\rangle^* \right) a_p^\dagger - \mathrm{H.c.}, \rho_p(t) \right] + \gamma_p \mathcal{D}_{a_p}\rho_p(t),$$
$$\dot\rho_s(t) = \frac{\chi}{2}\left[ \langle a_p\rangle a_s^{\dagger\,2} - \mathrm{H.c.}, \rho_s(t) \right] + \gamma_s \mathcal{D}_{a_s}\rho_s(t),$$
(10)

known as mean-field equations [50]. These equations are quadratic in the field operators and therefore it is straightforward to solve them either numerically for the dynamics or analytically for the fixed points [45,50]. The stationary state of the signal mode will be a Gaussian state [13–15] centered around a vanishing field amplitude $\langle a_s\rangle = 0$ as the mean-field equations do not break the Ising-type $Z_2$ symmetry. The steady state of the pump mode will be a coherent state with an amplitude given by $\langle a_p\rangle_{ss}^{MF} = (\epsilon_p - \frac{\chi}{2}\langle a_s^2\rangle_{ss}^{MF})/\gamma_p$.

Just like the c-MoP equations (4) and (5), the mean-field equations are coupled nonlinear equations which have to be solved self-consistently. Within mean-field theory, fluctuations of the pump mode are disregarded. Fluctuations of the signal mode, however, are (at least to some extent) taken into account [45,50]. This leads to the regularization of the divergences appearing in the classical theory or rather the standard linearization approach. For our purposes, it is important to note that the pump field amplitude always stays below the classical above-threshold solution, i.e., $\langle a_p\rangle_{ss}^{MF} < \gamma_s/\chi$. In the remainder of the paper, we will use it as the displacement in Eq. (3), i.e., $\tilde\alpha_p = \langle a_p\rangle_{ss}^{MF}$. This will guarantee a well-behaved Liouvillian for the free system $\mathcal{L}_s$, as we will explain in more detail in Sec. III B.

The mean-field equations can also be found by putting the factorized state ansatz $\rho(t) = \rho_p(t) \otimes \rho_s(t)$ into the Liouville–von Neumann equation, given by Eq. (1), before tracing out each of the modes separately. This well-known procedure, indeed, neglects all signal-pump correlations. Within the self-consistent projection operator theory, mean-field theory can be understood as an approximation to linear order in the interaction $\mathcal{L}_I$ for the dynamics of reduced density matrices. Our theory therefore provides a systematic generalization of mean-field approaches. It is due to the Born terms, which are second order in $\mathcal{L}_I$, that signal-pump correlations are taken into account. Therefore, we expect a higher quality of approximation by going from first order to second order in the interaction.

### B. Born terms

In order to solve the full c-MoP equations including the Born terms, we will need to overcome two main difficulties. While the c-MoP equation (5) of the pump mode is quadratic in the field operators, granting us a closed set of equations including only first and second moments of the pump field, the c-MoP equation (4) of the signal mode is quartic in the field operators. We will therefore either solve the latter fully numerically (see Sec. IV) or apply a *Gaussian state approximation*, as presented in Sec. V. In either of these two approaches, we need to overcome the second difficulty which arises due to the non-Markovian structure of our theory. In the remainder of this section, we will thus show how to rewrite the integrodifferential c-MoP equations (4) and (5) into a set of coupled ordinary differential equations. For the present problem, this step is crucial, as solving the integrodifferential equations is significantly more demanding for both numerical and analytical approaches.

We start by evaluating the correlation functions of the pump. By taking derivatives of the pump correlators $d_p^\pm(t,t')$ and $\tilde d_p^\pm(t,t')$ with respect to $t$ [see Eq. (8)], considering initial conditions at $t = t'$ (note that we understand from the c-MoP equations that $t' \leqslant t$), and exploiting the fact that the operator $\delta a_p^\dagger(t')\rho_p(t')$ is traceless, we find

$$d_p^+(t,t') = \tilde d_p^+(t,t') = \left[ \langle a_p^{\dagger\,2}\rangle(t') - \langle a_p\rangle^{*2}(t') \right] e^{-\gamma_p(t-t')},$$
$$\tilde d_p^-(t,t') = \left[ 1 + \langle a_p^\dagger a_p\rangle(t') - |\langle a_p\rangle(t')|^2 \right] e^{-\gamma_p(t-t')},$$
(11)
$$d_p^-(t,t') = \left[ \langle a_p^\dagger a_p\rangle(t') - |\langle a_p\rangle(t')|^2 \right] e^{-\gamma_p(t-t')}.$$

Hence, all correlation functions of the pump can be written in a form where the $t$ dependence only enters in a simple exponential factor.

A bit more effort is needed in order to simplify the correlation functions of the signal, but the main steps are mainly identical. All of the functions in Eq. (9) are of the form $f(t,t') = \mathrm{Tr}_s\{a_s^{\dagger\,2} e^{\mathcal{L}_s(t-t')}A(t')\}$ with a traceless operator $A(t')$ depending solely on $t'$. Again, we take the derivative of $f(t,t')$ with respect to $t$ and find an equation of motion of the form $\partial_t \vec v_{t'}(t) = M\vec v_{t'}(t)$ with a column vector

$$\vec v_{t'}(t) = \mathrm{col}\big(\widetilde{\langle a_s^\dagger a_s\rangle}, \widetilde{\langle a_s^2\rangle}, \widetilde{\langle a_s^{\dagger\,2}\rangle}\big),$$
(12)

where the expectation values with the tilde are defined in the usual way as the trace over the signal mode, but with a density matrix given by $\tilde\rho_{t'}(t) = e^{\mathcal{L}_s(t-t')}A(t')$. The matrix $M$ reads

$$M = \begin{pmatrix} -2\gamma_s & \chi\tilde\alpha_p & \chi\tilde\alpha_p^* \\ 2\chi\tilde\alpha_p^* & -2\gamma_s & 0 \\ 2\chi\tilde\alpha_p & 0 & -2\gamma_s \end{pmatrix}.$$

It is straightforward to diagonalize $M$. We write $M = U\Lambda U^{-1}$, with a similarity matrix $U$ that can be found analytically (but its expression is too lengthy to be reported here), and $\Lambda$ is the diagonal form of $M$ containing its eigenvalues $\lambda_1 = -2\gamma_s$ and $\lambda_{2,3} = -2\gamma_s \mp 2\chi|\tilde\alpha_p|$. We now

solve for the vector $\vec{v}_{t'}(t)$ to find

$$\vec{v}_{t'}(t) = U e^{\Lambda(t-t')} U^{-1} \vec{v}_{t'}(t') \equiv \sum_{n=1}^{3} e^{\lambda_n(t-t')} M_n \vec{u}_{A(t')}, \quad (13)$$

where we have defined the initial condition vector

$$\vec{u}_{A(t')} = \vec{v}_{t'}(t') = \begin{pmatrix} \mathrm{Tr}_s\{a_s^\dagger a_s A(t')\} \\ \mathrm{Tr}_s\{a_s^2 A(t')\} \\ \mathrm{Tr}_s\{a_s^{\dagger 2} A(t')\} \end{pmatrix}, \quad (14)$$

and the matrices $M_n = U \Pi_n U^{-1}$, where $\Pi_n$ is a projector in the $n$th "direction," that is, a matrix with zeros everywhere but in element $(n,n)$ which is one. Note that for the limit $\lim_{t\to\infty} \vec{v}_{t'}(t)$ to be uniquely defined, and therefore for $\mathcal{L}_s$ to be well behaved, all the eigenvalues of $M$ must satisfy $\mathrm{Re}\{\lambda_n\} < 0$, which in turn leads to a requirement for the displacement $\chi \tilde{\alpha}_p < \gamma_s$. This requirement is indeed fulfilled by choosing the mean-field displacement as mentioned above; see Sec. III A. In contrast, taking the classical solution as the displacement would lead to an ill-behaved $\mathcal{L}_s$ above and at the classical threshold point, that is, for $\sigma \geqslant 1$.

Coming back to the correlation functions in Eq. (9), the general solution (13) allows us to write them all as

$$d_s(t,t') = \sum_{n=1}^{3} e^{\lambda_n(t-t')} d_{s,n}(t'), \quad (15)$$

with $d_{s,n}(t) = [M_n \vec{u}_{A(t)}]_3$ (the subscript denoting the third vector component), where $d_s$ denotes any of the correlation functions $\{d_s^+, \tilde{d}_s^+, d_s^-, \tilde{d}_s^-\}$ for which $A$ is taken, respectively, as $\{\delta a_s^{\dagger 2}\rho_s, \rho_s \delta a_s^{\dagger 2}, \delta a_s^2 \rho_s, \rho_s \delta a_s^2\}$. Let us emphasize that just as with the pump mode, we have been able to write all of the correlation functions of the signal mode into a form where the $t$ dependence only enters in simple exponential factors.

Finally, let us show how this form for the correlation functions allows us to turn the c-MoP equations, which are coupled integrodifferential equations, into coupled ordinary differential equations. For this aim, let us rewrite Eqs. (4) and (5) as

$$\dot{\rho}_s(t) = \mathcal{L}_s \rho_s(t) + \frac{\chi}{2} \left[ a_s^{\dagger 2} \langle a_p \rangle(t) - a_s^2 \langle a_p \rangle^*(t), \rho_s(t) \right]$$
$$+ \left( \frac{\chi}{2} \right)^2 \left\{ \left[ a_s^2, h_s(t) \right] + \mathrm{H.c.} \right\}, \quad (16)$$

$$\dot{\rho}_p(t) = \mathcal{L}_p \rho_p(t) + \frac{\chi}{2} \left[ a_p \langle a_s^2 \rangle^*(t) - a_p^\dagger \langle a_s^2 \rangle(t), \rho_p(t) \right]$$
$$+ \left( \frac{\chi}{2} \right)^2 \left\{ \left[ a_p, \sum_{n=1}^{3} h_{p,n}(t) \right] + \mathrm{H.c.} \right\}, \quad (17)$$

where we have defined the operators

$$h_s(t) = \int_0^t dt' e^{\mathcal{L}_s(t-t')} \mathcal{K}_s(t,t') \rho_s(t'),$$
$$h_{p,n}(t) = \int_0^t dt' e^{\mathcal{L}_p(t-t')} \mathcal{K}_{p,n}(t,t') \rho_p(t'), \quad (18)$$

with the superoperator $\mathcal{K}_{p,n}$ defined as $\mathcal{K}_p$ in Eq. (7), but with the correlation functions $d_{s,n}(t)$ instead of $d_s(t)$. Using their definition and the solutions found for the correlation functions

given by Eqs. (11) and (15), their evolution equations are found to be

$$\partial_t h_s(t) = (-\gamma_p + \mathcal{L}_s) h_s(t) + \mathcal{K}_s(t,t) \rho_s(t), \quad (19)$$

$$\partial_t h_{p,n}(t) = (\lambda_n + \mathcal{L}_p) h_{p,n}(t) + \mathcal{K}_{p,n}(t,t) \rho_p(t). \quad (20)$$

Together with Eqs. (16) and (17), these form a closed set of coupled nonlinear ordinary differential equations for the reduced states $\rho_s$ and $\rho_p$, and the traceless operators $h_s$ and $\{h_{p,n}\}_{n=1,2,3}$. These are the equations that we analyze in the remainder of the paper.

Overall we have shown for the example of the DOPO that it is indeed possible to rewrite the integrodifferential c-MoP equations into a set of ordinary differential equations. The steps presented here are quite general and can be pursued for all c-MoP equations describing any physical system. The complexity of the resulting set of coupled equations will depend on the complexity of the subparts of the full quantum system, here given by the complexity of $\mathcal{L}_p$ and $\mathcal{L}_s$.

Finally, we remark that the c-MoP equations preserve the trace and the Hermiticity but they do not guarantee the positivity of the density matrix. Such an issue is not unusual for projection operator theories; in fact, the same conditions can be found in the well-established Redfield equations [51,52]. Obviously, whenever the c-MoP equations provide a good approximation, they will yield a positive density matrix. Hence the positivity of the eigenvalues can be used as a consistency test for the approximation.

### C. The adiabatic and the diabatic limit

In standard open system theory, one relies on a separation of time scales between the system dynamics and the environment correlations. A similar reasoning is applied in adiabatic elimination approaches, where in the case of the DOPO one relies on a separation between the rates $\gamma_p$ and $\gamma_s$ at which the pump and the signal, respectively, relax to the steady state of their unperturbed Liouvillians $\mathcal{L}_p$ and $\mathcal{L}_s$. The c-MoP theory can, in fact, be understood as a generalization of adiabatic elimination procedures where one considers the backaction of the system onto the environment. We will now show that the effective equations for the reduced state of the signal known in the *adiabatic* [17] and the *diabatic* [50] limit s can, indeed, be obtained as limiting cases of the c-MoP equations.

The adiabatic limit in which the time scale of the pump mode is much faster than the time scale of the signal mode is defined such that $\gamma_p/\gamma_s \to \infty$, while $\gamma_s \gamma_p$ is kept finite. The diabatic limit describes the opposite scenario where $\gamma_p/\gamma_s \to 0$. We proceed by comparing the Born terms with the free evolution operators $\mathcal{L}_p$ and $\mathcal{L}_s$, for which we consider the scaling of $h_s/\gamma_s$ and $h_{p,n}/\gamma_p$, which can be obtained by simple inspection of Eqs. (19) and (20) divided by $\gamma_s$ and $\gamma_p$, respectively. In the adiabatic limit, we infer from Eq. (20)/$\gamma_p$ that $h_{p,n}(t)/\gamma_p = 0$ for all $n$ and $t \geqslant 0$. Introducing this result into Eq. (17), we see that the state of the pump will be coherent with a field amplitude obeying the equation of motion,

$$\partial_t \langle a_p \rangle = \epsilon_p - \gamma_p(\langle a_p \rangle + \tilde{\alpha}_p) - \frac{\chi}{2} \langle a_s^2 \rangle. \quad (21)$$

On the other hand, Eq. (19)$/\gamma_s$ leads to $h_s(t)/\gamma_s = \mathcal{K}_s(t,t)/\gamma_s\gamma_p = \rho_s(t)\delta a_s^{\dagger 2}(t)/\gamma_s\gamma_p$, where we have used Eqs. (6) and (11) and the fact that when the pump is in a coherent state all the expectation values in Eq. (11) cancel. Introducing this result into Eq. (16), together with the steady-state solution of Eq. (21) for $\langle a_p \rangle$, we end up with the effective master equation of the signal mode in the adiabatic limit,

$$\gamma_s^{-1}\partial_t\rho_s = \frac{\sigma}{2}\left[a_s^{\dagger 2} - a_s^2, \rho_s\right] + \frac{g^2}{4}\mathcal{D}_{a_s^2}\rho_s + \mathcal{D}_{a_s}\rho_s, \quad (22)$$

where $\sigma = \epsilon_p\chi/\gamma_p\gamma_s$ is an injection parameter corresponding to a coherent exchange of excitations between the signal and pump modes, while $g^2 = \chi^2/\gamma_p\gamma_s$ accounts for signal photon pairs that are lost to the strongly damped pump mode. Equation (22) has been extensively studied in the literature [32,33,53]. It can be derived via standard adiabatic elimination which in the language of projection operator theory uses a time-independent projection superoperator $\mathcal{P}_{ad}$ projecting out the coherent laser field [17]. Its action on the full density matrix is given by $\mathcal{P}_{ad}\rho(t) \equiv |\alpha\rangle\langle\alpha| \otimes \rho_s(t)$, where $|\alpha\rangle$ is a coherent state with $\alpha = \epsilon_p/\gamma_p$. The fast exponential decay $e^{-\gamma_p(t-t')}$ of the pump correlation functions allows in this case for a Markovian approximation in the Born terms, that is, $\int_0^t dt' e^{\mathcal{L}_s(t-t')}\mathcal{K}_s(t,t')\rho_s(t') \approx \mathcal{K}_s(t,t)\rho_s(t)/\gamma_p$.

Let us now analyze the c-MoP equations in the diabatic limit. In this case, Eq. (19)$/\gamma_s$ provides us with $h_s(t)/\gamma_s = 0$, which, when introduced in Eq. (16), leads to an effective master equation,

$$\dot{\rho}_s(t) = \frac{\chi}{2}\left[\langle a_p \rangle a_s^{\dagger 2} - \langle a_p \rangle^* a_s^2, \rho_s(t)\right] + \mathcal{D}_{a_s}\rho_s(t), \quad (23)$$

for the signal state. The pump state only enters this equation through the amplitude $\langle a_p \rangle$ which obeys Eq. (21) since $h_{p,n}$ is traceless. Noting that this equation is equivalent to Eq. (10), we conclude that the diabatic limit reduces the full c-MoP equations to the mean-field equations.

We emphasize that within these limits, both Eqs. (10) and (22) become exact. We have thus shown that the c-MoP theory provides us with exact equations of motion in the limits $\gamma_p/\gamma_s \rightarrow \infty$ (adiabatic) and $\gamma_p/\gamma_s \rightarrow 0$ (diabatic) where it therefore becomes equivalent to well-established theories [17,50]. In the remainder of the paper, we will step beyond these cases in which time-scale separation is present and use the c-MoP theory to access the signal state in the $\gamma_p \approx \gamma_s$ scenario.

## IV. ACCURACY TESTS AND FULL QUANTUM STATES OF THE SIGNAL MODE

In the previous section, we have shown how to deal with the non-Markovian structure of the c-MoP equations. The only remaining difficulty is given by the quartic structure of the effective equations of motion derived for the signal mode, given by Eqs. (16) and (19). In this section, we will treat the problem numerically in the Fock state basis by introducing a truncation $D_s$ for the Hilbert space $\mathcal{H}_s$ of the signal, where $D_s$ is chosen such that the results for the observables we are interested in converge up to some desired accuracy. Thus, the reduced state $\rho_s$ and the operator $h_s(t)$ will be $D_s \times D_s$ dimensional matrices. Instead of treating the pump mode in an

analogous manner, we exploit the fact that the c-MoP equations of the pump mode (17) and (20) are quadratic in the bosonic operators. As a consequence, we are able to describe the pump state by a set of closed equations for five variables only, the mode amplitude $\langle a_p \rangle$ plus the fluctuations $\langle a_p\delta a_p \rangle$ and $\langle a_p^{\dagger}\delta a_p \rangle$ (note that the first two are complex variables). At the end, we are thus effectively left with two coupled differential equations for the matrices $\rho_s(t)$ and $h_s(t)$, with the pump equations solved either in parallel numerically or analytically as a function of signal observables.

In th e following, we compare the steady states of the classical theory from Eq. (2), the steady states of the mean-field equations (10), and the steady states of the c-MoP equations. In order to show the accuracy of the latter, we also determine the steady state of the full Liouville–von Neumann equation (1) in parameter regimes where it is numerically tractable. This numerical simulation is done as follows: first, we eliminate the large coherent background of the laser drive from the Liouvillian $\mathcal{L}$ by writing $a_p = \alpha_p + \delta a_p$, where $\alpha_p$ is taken to be the classical steady-state solution of Eqs. (2); then, we use the superspace formalism, where the steady-state operator $\rho_{ss}$ and the Liouville superoperator $\mathcal{L}$ are represented, respectively, by a vector $\vec{\rho}_{ss}$ and a matrix $\mathbb{L}$, and $\vec{\rho}_{ss}$ can be found as the eigenvector with zero eigenvalue of $\mathbb{L}$ [53,54]. As the dimension of the matrix $\mathbb{L}$ is $(D_p \times D_s)^2$, with $D_p$ denoting the pump mode's Hilbert-space dimension, this exact simulation is limited to small photon numbers.

In all of the simulations, we consider cases without time-scale separation between the two modes and rescale all units to the dissipation rates, i.e., we put $\gamma_p = \gamma_s = 1$. The only remaining parameters are the nonlinear coupling $\chi$ and the injection parameter $\sigma = \epsilon_p\chi$.

In Fig. 2, we present results in parameter regimes where the full DOPO equation (1) can be solved numerically. In Figs. 2(a)–2(c) and 2(d)–2(f), we show different steady-state observables for $\chi = 1$ and $\chi = 0.1$, respectively. It can be appreciated how the c-MoP results (blue solid line) coincide almost perfectly with the numerical results from the full master equation (red stars). The observables that we show are the pump mode's amplitude $\langle a_p \rangle$ in Figs. 2(a) and 2(d), the signal photon number $\langle a_s^{\dagger}a_s \rangle$ in Figs. 2(b) and 2(e), and the $g^{(2)}$ function $g_s^{(2)}(0) \equiv \langle a_s^{\dagger 2}a_s^2 \rangle/\langle a_s^{\dagger}a_s \rangle^2$ of the signal in Figs. 2(c) and 2(f). We also compare with the mean-field predictions of Eq. (10) (black dashed line), which in this context should be understood as the c-MoP theory up to first order, and with the classical steady-state solutions (gray thin solid line) given after Eq. (2). Let us remark that despite the nonlinear nature of the mean-field and the c-MoP equations, we only find one physical solution for each of them.

All four theories agree quite well far below the critical point $\sigma = 1$ as the states of the signal and pump modes are close to vacuum and a coherent state induced by the external laser drive, respectively. Far above the threshold point, where the classical theory is expected to be approximately valid, we find that both the c-MoP predictions and the full numerics agree well with the classical solutions for all observables, but with the fundamental difference that the classical theory breaks the $Z_2$ symmetry, while c-MoP and the full solution preserve it. The mean-field solution, on the other hand, fails to describe the
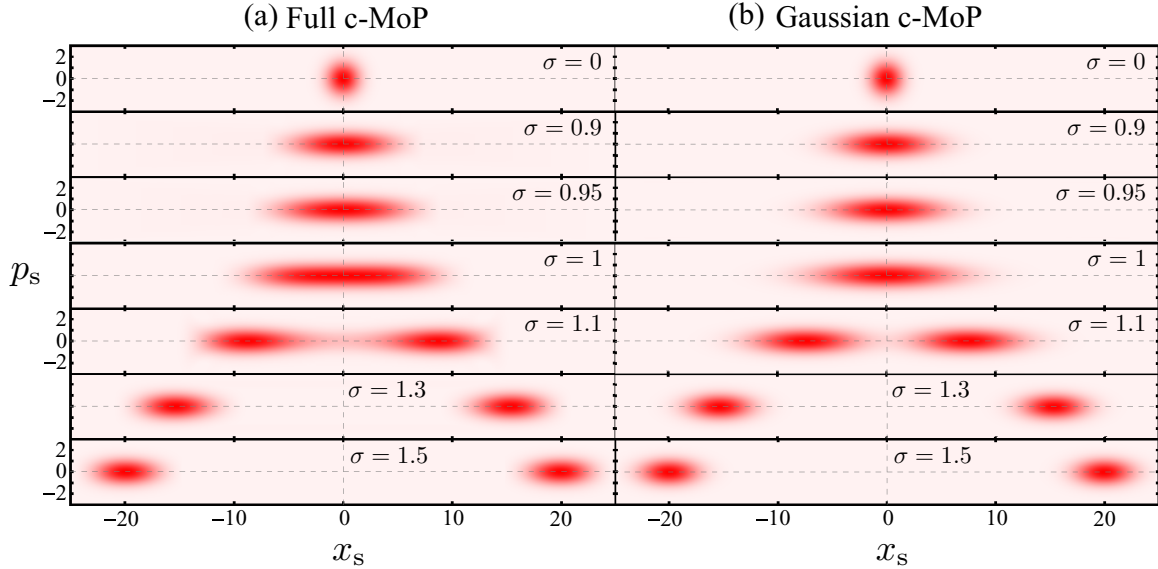
FIG. 3. (Color online) Wigner functions of the c-MoP density matrix for the signal mode (a) without and (b) with the Gaussian state approximation for $\gamma_p = \gamma_s = 1$, $\chi = 0.1$, and for different values of $\sigma$. In the absence of injection, $\sigma = 0$, the signal state is in vacuum, and one finds the characteristic uncertainty circle showing the same quantum noise in any direction of phase space. Upon approaching the threshold, the state becomes squeezed, with the highest squeezing levels obtained around $\sigma = 1$, what can be appreciated by the clear gap present between the end of the uncertainty region and the frame along the $p$ axis, in contrast to the $\sigma = 0$ case where the uncertainty region is almost touching the frame. Above threshold, two symmetric peaks appear and the squeezing reaches some asymptotic value as we move away from threshold. Note how above threshold the state can be approximated by a balanced mixture of two symmetry-breaking states. Indeed, let us remark that while for $\sigma < 1$ we are plotting the unique solution that appears when applying the Gaussian state approximation onto the c-MoP equations (which we have called below-threshold solution in the text), for $\sigma > 1$ we have chosen to plot the Wigner function corresponding to a balanced mixture of the two above-threshold symmetry-breaking solutions with opposite phase which coexist with the symmetry-preserving Gaussian solution.

state of the signal above threshold, as can be appreciated from the $g^{(2)}$ function in Figs. 2(c) and 2(f). As expected, mean-field theory and the classical theory break down in the vicinity of the threshold point. Remarkably, this is not true for c-MoP which appears to give quasiexact results for all values of $\sigma$, even in cases where the interaction rate $\chi$ is comparable to all other system parameters.

For the experimentally relevant scenario with $\chi \ll 1$, the Hilbert-space dimension needs to be so large that we are not able to find the numerical solution of the full master equation (1) for injection parameters close to (or above) threshold. However, we can compare the c-MoP predictions (red stars) [see Fig. (4)] with the perturbative approach which Drummond *et al.* (dark yellow dot-dashed line) developed in the vicinities of the critical point by making a consistent multiple-scale expansion of the system's stochastic variables within the positive $P$ representation [36,37]. This procedure has the virtue of being valid for any values of $\gamma_p$ and $\gamma_s$ and close to threshold, concretely for $|\sigma - 1| < \chi/\sqrt{2\gamma_p\gamma_s}$, it is expected to be quasiexact. As shown in Figs. 4(a) and 4(b), we find perfect agreement between this approach and the c-MoP theory for $\chi = 0.01$.

Overall, we have indeed shown the drastic impact of the Born terms, which do not only lead to a quantitative improvement as compared to the classical theory or to mean-field theory, but to a qualitatively different state of the signal mode. The classical theory predicts a coherent state, while the mean-field theory, i.e., the c-MoP theory up to

first order, predicts a Gaussian state of the signal centered around $\langle a_s \rangle = 0$ [45]. The c-MoP theory including the Born terms; hence including signal-pump correlations within a projection-operator-based theory is capable of finding the full quantum state of the signal which is neither coherent nor Gaussian, as shown through the $g^{(2)}$ function in Figs. 2(c) and 2(f).

In order to illustrate the full quantum state, we plot the Wigner function $W(x_s, p_s)$ of the signal density matrix obtained from the c-MoP equations in Fig. 3(a) for $\chi = 0.1$ and different values of $\sigma$. Let us remark that in our case in which the Wigner function is positive everywhere in the phase space formed by the quadratures $x_s = a_s^\dagger + a_s$ and $p_s = i(a_s^\dagger - a_s)$, it can be simply interpreted as the joint probability distribution describing the statistics of measurements of these observables [13–15]. From a computational point of view, we evaluate it from the steady-state density matrix following the method detailed in [55]. Far below threshold, the Wigner function shows a perfect vacuum for the signal state; see top panel of Fig. 3(a) for $\sigma = 0$ as a reference. As we cross through the critical point, two significant effects take place. First, approaching the threshold, we find the well-known quadrature-noise reduction or *squeezing* [5,17,56,57], which is highest, albeit only 50% that of the vacuum noise level, around the critical point $\sigma = 1$ [37,45] and reaches its asymptotic value $\langle \delta p_s^2 \rangle = (\gamma_s + \gamma_p)/(2\gamma_s + \gamma_p)$ for $\sigma \to \infty$ [45]. Second, as we cross the threshold, we appreciate how the state develops two lobes centered close to the quadrature values predicted by the

classical solution, each reaching the asymptotic value of the squeezing mentioned before for $\sigma \to \infty$, with corresponding *antisqueezing* $\langle \delta x_s^2 \rangle = 1 + \gamma_s/\gamma_p$ [45]. Hence, even though the true quantum state always preserves the $Z_2$ symmetry, it does so in two qualitatively different ways depending on whether we are below or above threshold. This behavior is reminiscent of the one appearing in the adiabatic limit [17,32,33] and has been recently observed by making use of a circuit QED architecture [58].

In retrospect, we see that the symmetry-breaking states predicted above threshold by the standard linearization approach each correspond to one of the two distinct peaks appearing in the exact state. Far above threshold, $\sigma \gg 1$, the two peaks have zero overlap and such states provide reasonable predictions for all observables which are not sensitive to symmetry breaking, that is, all observables containing even numbers of signal field operators. Of course, such a deficit can be corrected by simply using a balanced mixture of the symmetry-breaking states [45]; this construction will guide us in the next section, where we will perform a Gaussian state approximation which necessarily breaks the $Z_2$ symmetry. It is then close to the critical point where both linearization and mean-field approaches fail, whereas c-MoP provides an accurate description of the quantum state.

Let us remark that we have compared the Wigner function obtained from the c-MoP theory with the reduced signal states obtained from the full master equation, which was only possible for $\sigma \leqslant 1.2$, and found very good agreement, with the differences being completely unnoticeable to the naked eye. We emphasize again that with the numerical solution of the c-MoP equations, we are able to find the full reduced density matrices of the modes away from the adiabatic limit. This is in contrast to other approaches such as stochastic simulations [36–39] or the Keldysh formalism [40–42], which are naturally designed to provide expectation values of the system operators.

## V. GAUSSIAN STATE APPROXIMATION WITHIN THE C-MOP THEORY

Despite the fact that the complexity of solving the c-MoP equations fully numerically scales in a more favorable way than the numerical complexity of the full master equation, it still requires integration of a number of differential equations that scales quadratically with the dimension of the truncated Hilbert space for the signal field. Therefore, it is very desirable to find an effective description of the underlying theory which is numerically more efficient and can thus cover the whole parameter space. In the remainder of this section, we implement such an idea by applying a Gaussian state approximation (GSA) consistent with the c-MoP equations (4) and (5).

Another great advantage of a Gaussian theory, apart from reaching the whole parameter space, is the efficiency in the evaluation of both steady states and dynamical quantities such as two-time correlation functions. The disadvantage of a Gaussian theory, however, is the lack of quantitative accuracy especially in the vicinity of the critical point. Nonetheless, as we show in the following, a Gaussian theory consistent with the c-MoP equations offers better quantitative accuracy than any of the previously developed Gaussian methods, particularly

linearization around the classical solution or the recently developed self-consistent linearization [45].

The general procedure for finding a GSA for the state of a certain bosonic master equation is very simple. In a first step, we write the bosonic operators as $a_j = \alpha_j + \delta a_j$, with $\alpha_j = \langle a_j \rangle$, such that $\langle \delta a_j \rangle = 0$. In the next step, we find the evolution equation for the first and second moments, which will depend on higher-order moments in general. Thus, in the final step, we assume the state to be Gaussian at all times, so that all higher-order moments factorize into products of first- and second-order moments [17,45]; in particular, we will encounter third-order moments such as, e.g., $\langle \delta a_s^{\dagger 2} \delta a_s \rangle$, which vanish identically within the GSA, and fourth-order moments which factorize according to, e.g.,

$$
\begin{aligned}
\langle \delta a_s^{\dagger 4} \rangle &\approx 3 \langle \delta a_s^{\dagger 2} \rangle^2, \\
\langle \delta a_s^{\dagger 3} \delta a_s \rangle &\approx 3 \langle \delta a_s^{\dagger 2} \rangle \langle \delta a_s^{\dagger} \delta a_s \rangle, \\
\langle \delta a_s^{\dagger 2} \delta a_s^2 \rangle &\approx \langle \delta a_s^{\dagger 2} \rangle \langle \delta a_s^2 \rangle + 2 \langle \delta a_s^{\dagger} \delta a_s \rangle^2.
\end{aligned}
\tag{24}
$$

After this final step, we are then left with a closed set of nonlinear equations for the amplitudes $\alpha_j$ and the second-order moments of the fluctuations $\delta a_j$ that have to be solved self-consistently.

The standard linearization theory can be understood as a GSA on the full master equation, but with the exception that the amplitudes $\alpha_j$ are not determined self-consistently, but are obtained from the classical theory. As shown by the gray thin solid line in Fig. 4(b), the complete suppression of quantum fluctuations when determining these amplitudes leads to unphysical results at the threshold point in the DOPO.

The self-consistent linearization method, as it is coined in Ref. [45], goes one step beyond standard linearization by consistently finding the amplitudes $\alpha_j$ from the GSA still applied to the full master equation. Due to the nonlinear nature of the resulting equations of motion, one can find several solutions in a given point of parameter space. However, it was shown that at the end, only two types of solutions were physical, qualitatively similar to the solutions found from standard linearization, but quantitatively regularized in such a way that the unphysical results of the latter disappear. In particular, a below-threshold (BT) solution was found, which does not break the $Z_2$ symmetry, i.e., $\alpha_s = 0$, but in contrast to the classical theory exists for all values of the injection parameter, not only for $\sigma < 1$. We also found two above-threshold (AT) solutions with opposite phase, which break the symmetry, that is, $\langle a_s \rangle = \pm|\alpha_s| \neq 0$, but appear only above a certain injection parameter $\sigma > 1$ which is larger than the classical threshold value. Interestingly, we point out that the BT solution found through this self-consistent linearization is exactly equivalent to the mean-field theory introduced in Sec. III A.

Motivated by these findings, we apply a GSA to the c-MoP equations. Concretely, we calculate all first- and second-order moments of the pump and signal fluctuations from the c-MoP equations (16), (17), (19), and (20), and apply the factorization of higher-order moments as explained above. In strong contrast to the GSA on the full master equation, we do not need to assume a Gaussian form for the full state $\rho$, but only for
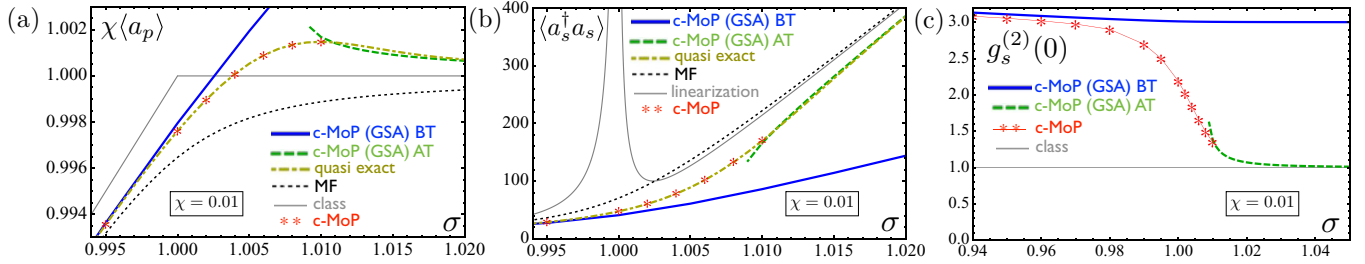
FIG. 4. (Color online) Accuracy tests of the c-MoP theory with and without the Gaussian state approximation for steady-state observables as a function of the injection $\sigma$. In all of the plots, we set $\gamma_p = \gamma_s = 1$ and $\chi = 0.01$. As in Fig. 2, we show (a) the rescaled pump field amplitude $\chi\langle a_p \rangle$, (b) the signal photon number $\langle a_s^\dagger a_s \rangle$, and (c) the $g^{(2)}$ function of the signal. The red stars show the results obtained from the c-MoP equations (16), (17), (19), and (20), up to injection parameters $\sigma$ where the numerics are tractable. For comparison, the quasiexact method of Drummond and collaborators [36,37] is shown as a dark yellow dot-dashed line. The blue solid and the green dashed curves represent the below- and above-threshold solutions, respectively, obtained from a Gaussian state approximation on the c-MoP equations. The black thin dotted curve displays the results of mean-field theory [see Eq. (10)], which in this context can be understood as the below-threshold solution of a Gaussian state approximation on the full master equation (1). Finally, the gray thin solid lines represent the prediction of the standard linearization theory in (a) and (b), and the coherent-state prediction $g^{(2)} = 1$ of the classical equations (2) in (c).

the reduced state of the signal $\rho_s$. Hence, we expect similar qualitative results but with a higher quantitative accuracy.

Indeed, this is what we find and illustrate in Fig. 4 for $\gamma_p = \gamma_s = 1$ and $\chi = 0.01$. We plot steady-state expectation values for the pump amplitude $\chi\langle a_p \rangle$ in Fig. 4(a), the signal photon number $\langle a_s^\dagger a_s \rangle = \langle \delta a_s^\dagger \delta a_s \rangle + |\alpha_s|^2$ in Fig. 4(b), and the $g^{(2)}$ function of the signal in Fig. 4(c), all as a function of the injection parameter $\sigma$. The blue solid line shows the below-threshold solution of the GSA on the c-MoP equation, while the green dashed line illustrates the above-threshold solution. The latter fulfills $\langle \delta a_s^\dagger \delta a_s \rangle \ll |\alpha_s|^2$ and is therefore more likely to provide physically consistent results than the BT solution whenever they coexist. In Fig. 4(c), we show how the AT solution indeed gives the correct value for the $g^{(2)}$ function, what indicates that each of the AT solutions corresponds to one of the lobes of the Wigner function; see Fig. 3(a). In order to illustrate this point even further, we show in Fig. 3(b) the Wigner function [13–15] corresponding to the GSA on the c-MoP equations (as explained in the previous section, above threshold we take the balanced mixture of the two symmetry-breaking solutions, such that the resulting state preserves the $Z_2$ symmetry).

Importantly, there is an increased quantitative accuracy of the BT solution obtained from the c-MoP theory as compared with the mean-field theory (or the self-consistent linearization) [see Figs. 4(a) and 4(b)] for parameters below and especially at the classical threshold point. As mentioned in Sec. IV, we test the accuracy of our method by comparing with the quasiexact method of Drummond and collaborators [36,37], illustrated by the dark yellow dot-dashed line in Figs. 4(a) and 4(b). This increase in accuracy can be attributed to the Born terms, since the mean-field equations can be understood, on the one hand, as the first-order approximation of the c-MoP theory and, on the other hand, as the below-threshold solution of the GSA on the full master equation of the DOPO.

To summarize this section, we have shown that the c-MoP equations also provide a highly accurate Gaussian theory which is still as effective as every other linearized theory but, in contrast, it takes significant signal-pump correlations into account. This is relevant because, as stated above, a

Gaussian theory has the virtue that both steady-state as well as dynamical quantities such as two-time correlation functions can be found efficiently for any time and set of parameters. To emphasize this practical aspect of the GSA, we will show in Sec. VI that the level of accuracy that we have found here in the evaluation of the steady states is also present in the transient-time evolution.

## VI. DYNAMICS

So far we have only presented steady-state quantities for the various methods of our interest. In this section, we will briefly elaborate on the possibility to simulate dynamical evolution as well. The steady state of the full master equation (1) can be understood as an eigenvector corresponding to the zero eigenvalue of the Liouvillian $\mathcal{L}$ such that $\mathcal{L}\rho_{ss} = 0$. The formal solution for the time-evolving state which can be written as $\rho(t) = e^{\mathcal{L}t}\rho(0)$, on the other hand, involves all eigenvalues of the Liouvillian. Hence, it is *a priori* not clear whether a given approximate method used for the evaluation of the steady state of $\mathcal{L}$ will provide the same degree of accuracy when used for transient-time evolution.

In order to investigate this open issue, we simulate the time dynamics of the various approximate methods that we have introduced and compare their results with an exact simulation of the full master equation (1) in regions of the parameter space where it is numerically tractable. We analyze a situation in which the input laser drives the system from the initial vacuum to its steady state. Figure 5 shows the signal photon number as a function of time at the classical threshold point $\sigma = 1$, for $\gamma_p = \gamma_s = 1$, and for $\chi = 0.1$ in Fig. 5(a) and $\chi = 0.05$ in Fig. 5(b). The red stars in Fig. 5(a) illustrate the result obtained from the numerical simulation of the full master equation (1), while the red line in Fig. 5(b) illustrates the steady-state value of its observables only, since the small value of $\chi$ prevented us from being able to simulate the whole dynamics in this case. On the other hand, the blue solid curves represent the results obtained from the numerical integration of the c-MoP equations as explained in Sec. IV. Finally, the green dashed and black dotted lines represent the time evolution obtained from
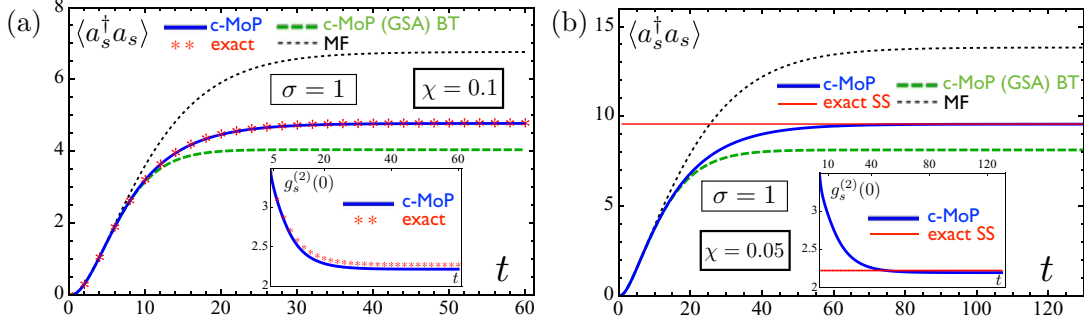
FIG. 5. (Color online) Accuracy tests of the c-MoP theory for transient-time evolution. The initial state is chosen to be the vacuum. We set $\gamma_p = \gamma_s = 1$, investigate the classical threshold point $\sigma = 1$, and choose (a) $\chi = 0.1$ and (b) $\chi = 0.05$. The plots display the signal photon number as a function of time in units of the dissipation rates, while the insets show the $g^{(2)}$ function of the signal mode. The red stars in (a) show the result obtained from the numerical simulation of the full master equation (1), while the red line in (b) indicates its steady-state values only. The blue solid curves represent the results obtained from the numerical integration of the c-MoP equations (16), (17), (19), and (20). Finally, the green dashed and black dotted lines represent the time evolution obtained from a Gaussian state approximation on the c-MoP equations and the full master equation (mean field), respectively.

a GSA on the c-MoP equations and the full master equation, respectively.

Remarkably, Fig. 5(a) shows that the level of accuracy found dynamically for the various approximations is similar to the ones that we already encountered when evaluating steady-state quantities. In particular, it is apparent that at any point in time, the GSA on the full master equation (mean field) is less accurate than the GSA on the c-MoP equations, which in turn does not have the remarkable level of accuracy shown by the full c-MoP numerical simulation, almost coinciding with the numerics of the full master equation at all times. It is important to note that the evolution of the $g^{(2)}$ function shown in the inset of Fig. 5(a) suggests that, indeed, the c-MoP equations are able to map the full quantum state of the signal in the course of time. Thus, the c-MoP theory provides an efficient approach for the investigation of the transient-time evolution in a driven-dissipative scenario, where quantum states in the intermediate time are expected to find practical applications for quantum engineering and computing [58].

A numerical simulation for the parameter set chosen in Fig. 5(b) demands minimal Hilbert-space dimensions of $\dim \mathcal{H}_p = 6$ and $\dim \mathcal{H}_s = 120$ in order to reach convergence up to an accuracy of $10^{-2}$ for the relevant observables. Thus, while the c-MoP approach requires a simulation of a set of 28 811 coupled nonlinear differential equations, in the case of the full master equation one has to integrate 518 400 coupled linear differential equations, which has precluded us from being able to simulate the dynamics from it. Therefore, we only show steady-state observables of the full master equation for this case.

Figures 5(a) and 5(b) further illustrate the scaling of various quantities with the nonlinear coupling $\chi$ at the critical point. In particular, note how both the signal photon number and the time that the system needs to reach the steady state double when $\chi$ is reduced by half. The latter is known in the literature as *critical slowing down* [36], and just as the signal photon number, it was predicted to scale with $\chi^{-1}$ [33,36,40], in agreement with our c-MoP simulation. Hence, we can appreciate the practical use of a Gaussian theory by considering that to simulate an experimentally relevant

scenario where $\chi \ll 1$, dynamical quantities would require extremely long simulation times, which, as explained before, can be efficiently handled with a GSA on the c-MoP theory, but not by its full numerical simulation. As an example, we have checked that for $\chi = 0.01$, a GSA on the c-MoP equations requires a normalized time of approximately 300 to reach the steady state, again in agreement with the $\chi^{-1}$ scaling, as it can be appreciated in Fig. 5(a) that such time is about 10 times smaller for $\chi = 0.1$.

## VII. CONCLUSIONS AND OUTLOOK

In conclusion, we have exemplified the applicability of the self-consistent projection operator theory to nonlinear quantum optical systems on the case study of the degenerate optical parametric oscillator. Our theory generalizes mean-field approaches and, in particular, adiabatic elimination methods to settings without time-scale separation. The effective master equations can be solved efficiently despite their non-Markovian structure. We have demonstrated the high degree of accuracy of our method and revealed its capability to determine the exact quantum states below, at, and above the classical threshold for both the stationary limit and dynamical evolution.

In addition, we developed a linearized theory consistent with the self-consistent Mori-projector equations and showed its accuracy far beyond other known linearized approaches. We expect our Gaussian method to be particularly useful in the context of hybrid systems such as optomechanical parametric oscillators [27,28], where fields of quantum nature with no coherent background are coupled to mechanical elements. Some intriguing tasks for future research would include applying the c-MoP approach to investigate dynamical questions, e.g., investigate tunneling times between the two symmetry-breaking states in parameter regimes away from the adiabatic limit [53], simulate quantum quenches in a driven-dissipative scenario [59], and investigate the effect of small symmetry-breaking perturbations on both the dynamics and steady states.

[1] R. W. Boyd, *Nonlinear Optics* (Academic, New York, 2003).

[2] K. Staliunas and V. J. Sanchez-Morcillo, *Transverse Patterns in Nonlinear Optical Resonators* (Springer, New York, 2002).

[3] D. F. Walls and G. Milburn, *Quantum Optics* (Springer, New York, 2007).

[4] M. O. Scully and M. S. Zubairy, *Quantum Optics* (CUP, Cambridge, 1997).

[5] *Nonclassical Effects in Quantum Optics*, edited by P. Meystre and D. F. Walls (American Institute of Physics, New York, 1991).

[6] M. J. Hartmann and M. B. Plenio, Phys. Rev. Lett. **99**, 103601 (2007).

[7] F. G. S. L. Brandão, M. J. Hartmann, and M. B. Plenio, New J. Phys. **10**, 043010 (2008).

[8] C. Navarrete-Benlloch, Ph.D. thesis, Universitat de València, Valencia, Spain, 2011.

[9] K. Goda, O. Miyakawa, E. E. Mikhailov, S. Saraf, R. Adhikari, K. McKenzie, R. Ward, S. Vass, A. J. Weinstein, and N. Mavalvala, Nat. Phys. **4**, 472 (2008).

[10] H. Vahlbruch, S. Chelkowski, B. Hage, A. Franzen, K. Danzmann, and R. Schnabel, Phys. Rev. Lett. **95**, 211102 (2005).

[11] N. Treps, N. Grosse, W. P. Bowen, C. Fabre, H.-A. Bachor, and P. K. Lam, Science **301**, 940 (2003).

[12] N. Treps, U. Andersen, B. Buchler, P. K. Lam, A. Maitre, H.-A. Bachor, and C. Fabre, Phys. Rev. Lett. **88**, 203601 (2002).

[13] S. L. Braunstein and P. van Loock, Rev. Mod. Phys. **77**, 513 (2005).

[14] C. Weedbrook, S. Pirandola, R. Garcia-Patron, N. J. Cerf, T. C. Ralph, J. H. Shapiro, and S. Lloyd, Rev. Mod. Phys. **84**, 621 (2012).

[15] C. Navarrete-Benlloch, arXiv:1504.05270.

[16] H. J. Carmichael, *Statistical Methods in Quantum Optics 1* (Springer-Verlag, Berlin, 2002).

[17] H. J. Carmichael, *Statistical Methods in Quantum Optics 2* (Springer-Verlag, Berlin, 2008).

[18] H. Mori, Prog. Theor. Phys. **33**, 423 (1965).

[19] C. W. Gardiner and P. Zoller, *Quantum Noise* (Springer-Verlag, Berlin, 2004).

[20] P. Degenfeld-Schonburg and M. J. Hartmann, Phys. Rev. B **89**, 245108 (2014).

[21] M. D. Reid and P. D. Drummond, Phys. Rev. Lett. **60**, 2731 (1988).

[22] P. D. Drummond and M. D. Reid, Phys. Rev. A **41**, 3930 (1990).

[23] C. Navarrete-Benlloch, E. Roldán, and G. J. de Valcárcel, Phys. Rev. Lett. **100**, 203601 (2008).

[24] C. Navarrete-Benlloch, G. J. de Valcárcel, and E. Roldán, Phys. Rev. A **79**, 043820 (2009).

[25] L. Mandel and E. Wolf, *Optical Coherence and Quantum Optics* (Cambridge University Press, Cambridge, 1995).

[26] H.-P. Breuer and F. Petruccione, *The Theory of Open Quantum Systems* (Oxford University Press, Oxford, 2002).

[27] F. Jimenez and C. Navarrete-Benlloch, arXiv:1412.2521.

[28] X.-Y. Lü, Y. Wu, J. R. Johansson, H. Jing, J. Zhang, and F. Nori, Phys. Rev. Lett. **114**, 093602 (2015).

[29] Emanuele G. Dalla Torre, S. Diehl, M. D. Lukin, S. Sachdev, and P. Strack, Phys. Rev. A **87**, 023831 (2013).

[30] F. Dimer, B. Estienne, A. S. Parkins, and H. J. Carmichael, Phys. Rev. A **75**, 013804 (2007).

[31] H. Ritsch, P. Domokos, F. Brennecke, and T. Esslinger, Rev. Mod. Phys. **85**, 553 (2013).

[32] P. D. Drummond, K. J. McNeil, and D. F. Walls, J. Mod. Opt. **28**, 211 (1981).

[33] M. Wolinsky and H. J. Carmichael, Phys. Rev. Lett. **60**, 1836 (1988).

[34] P. D. Drummond and C. W. Gardiner, J. Phys. A **13**, 2353 (1980).

[35] P. Kinsler, M. Fernee, and P. D. Drummond, Phys. Rev. A **48**, 3310 (1993).

[36] P. Kinsler and P. D. Drummond, Phys. Rev. A **52**, 783 (1995).

[37] P. D. Drummond, K. Dechoum, and S. Chaturvedi, Phys. Rev. A **65**, 033806 (2002).

[38] S. Chaturvedi and P. D. Drummond, Eur. Phys. J. B **8**, 251 (1999).

[39] D. T. Pope, P. D. Drummond, and W. J. Munro, Phys. Rev. A **62**, 042108 (2000).

[40] O. Veits and M. Fleischhauer, Phys. Rev. A **55**, 3059 (1997).

[41] C. J. Mertens, T. A. B. Kennedy, and S. Swain, Phys. Rev. Lett. **71**, 2014 (1993).

[42] C. J. Mertens, T. A. B. Kennedy, and S. Swain, Phys. Rev. A **48**, 2374 (1993).

[43] L. A. Lugiato and G. Strini, Opt. Commun. **41**, 67 (1982).

[44] M. J. Collett and C. W. Gardiner, Phys. Rev. A **30**, 1386 (1984).

[45] C. Navarrete-Benlloch, E. Roldán, Y. Chang, and T. Shi, Opt. Express **22**, 024010 (2014).

[46] A. Rivas and S. F. Huelga, *Open Quantum Systems. An Introduction* (Springer, New York, 2011).

[47] S. G. Schirmer and Xiaoting Wang, Phys. Rev. A **81**, 062306 (2010).

[48] S. Gigan, L. Lopez, V. Delaubert, N. Treps, C. Fabre, and A. Maitre, J. Mod. Opt. **53**, 809 (2006).

[49] R. Zwanzig, *Nonequilibrium Statistical Mechanics* (Oxford University Press, Oxford, 2001).

[50] O. Veits and M. Fleischhauer, Phys. Rev. A **52**, R4344(R) (1995).

[51] A. G. Redfield, IBM J. Res. Dev. **1**, 19 (1957).

[52] K. Blum, *Density Matrix Theory and Applications* (Plenum, New York, 1981).

[53] P. Kinsler and P. D. Drummond, Phys. Rev. A **43**, 6194 (1991).

[54] C. Navarrete-Benlloch, arXiv:1504.05266.

[55] C. Navarrete-Benlloch, J. J. García-Ripoll, and Diego Porras, Phys. Rev. Lett. **113**, 193601 (2014).

[56] T. Eberle, S. Steinlechner, J. Bauchrowitz, V. Handchen, H. Vahlbruch, M. Mehmet, H. Muller-Ebhardt, and R. Schnabel, Phys. Rev. Lett. **104**, 251102 (2010).

[57] H. Vahlbruch, M. Mehmet, S. Chelkowski, B. Hage, A. Franzen, N. Lastzka, S. Gossler, K. Danzmann, and R. Schnabel, Phys. Rev. Lett. **100**, 033602 (2008).

[58] Z. Leghtas, S. Touzard, I. M. Pop, A. Kou, B. Vlastakis, A. Petrenko, K. M. Sliwa, A. Narla, S. Shankar, M. J. Hatridge, M. Reagor, L. Frunzio, R. J. Schoelkopf, M. Mirrahimi, and M. H. Devoret, Science **347**, 853 (2015).

[59] M. J. Bhaseen, J. Mayoh, B. D. Simons, and J. Keeling, Phys. Rev. A **85**, 013817 (2012).